Sparse Optimal Motor Estimation (SOME) for Extracting Commands for Prosthetic Limbs

Yao Li, *Member, IEEE*, Lauren H. Smith, Levi J. Hargrove *Member, IEEE*, Douglas J. Weber, *Member, IEEE*, and Gerald E. Loeb, *Senior Member, IEEE*

***Abstract*—It is possible to replace amputated limbs with mechatronic prostheses, but their operation requires the user's intentions to be detected and converted into control signals to the actuators. Fortunately, the motoneurons (MNs) that controlled the amputated muscles remain intact and capable of generating electrical signals, but these signals are difficult to record. Even the latest microelectrode array technologies and Targeted Motor Reinnervation (TMR) can provide only sparse sampling of the hundreds of motor units that comprise the motor pool for each muscle. Simple rectification and integration of such records is likely to produce noisy and delayed estimates of the actual intentions of the user. We have developed a novel algorithm for optimal estimation of motor pool excitation based on the recruitment and firing rates of a small number (2-10) of discriminated motor units. We first derived the motor estimation algorithm from normal patterns of modulated MN activity based on a previously published model of individual MN recruitment and asynchronous frequency modulation. The algorithm was then validated on a target motor reinnervation subject using intramuscular fine-wire recordings to obtain single motor units.**

***Index Terms* — Motor Neuron Pool, Sparse Estimation, Targeted Motor Reinnervation.**

I. Introduction

WHEN humans perform a motor task, the central nervous system (CNS) excites the alpha motoneurons (MNs) to activate the muscles, which in turn actuate the skeletal segments to perform the task. Each muscle consists of many fibers and is innervated by many alpha motoneurons (α-MNs), which are located in the spinal cord. When an α-MN sends an action potential to the muscle, the signal is received by a group of muscle fibers. Such a group–the motor unit (MU) – is generally recruited in order of ascending force-generating capability (the "size principle"), with each successive unit starting at a modest firing rate and increasing in frequency as the excitation of the MN pool (MNP) increases [1]. As excitatory input declines, or inhibitory input increases, α-MNs are generally de-recruited in order by size, from largest to smallest. The fine grading of force required for accuracy favors a design that allows both successive activation of the MNP and finely graded modulation of each active unit.

There are also correlations among MN size, the number and diameter of their innervated muscle fibers and various physiological properties [2]. For amputees, the motor pathway - from supraspinal structures to spinal cord to peripheral nerve - remains intact and capable of generating and transmitting electrical signals. The activity of surviving MNs can be recorded from the ventral horn, ventral roots [3,4] or peripheral nerves [5] to infer the prosthesis user's intentions and to control the prosthetic actuators (Fig.1), but only if the signals enable a rapid and accurate estimate of the excitatory drive to the MNP. However, even with the state-of-the-art microelectrode array technologies, only a few of the hundreds of MUs supplying each of the many amputated muscles (the MNP) are likely to be recorded [6, 7].

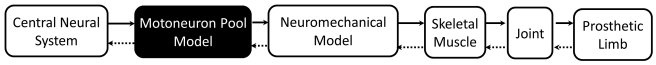

Figure 1. Stages of neural signal transmission for human motor control system. The design and operation of neural prostheses requires models that can be operated in both directions around this loop. In particular, when command signals are derived from neural activity (black box), they reflect an internal signal that arises from the middle of the loop, which must be worked backward to infer the user's intentions (our goal in this paper) and then forward to anticipate the consequences of delivering those commands to the prosthetic actuators.

In an early study from Hoffer et al [3, 4], a total of 150 fine flexible wire microelectrodes were implanted chronically in the fifth lumbar ventral root of 17 cats during locomotion on a treadmill. These microelectrodes yielded records of the natural discharge patterns of 164 individual axons, where only 51 axons were identified as MNs projecting to the anterior thigh muscle group (a given ventral root or peripheral nerve trunk normally innervates on the order of 10-20 functionally distinct muscles). For these axons, the centrifugal propagation of action potentials was demonstrated by the technique of spike-triggered averaging using signals recorded from cuff electrodes implanted around the femoral

Yao Li is with the Department of Biomedical Engineering, University of Southern California, Los Angeles, CA USA 90089 (Phone: +213-821-1114, Email: Yao.Li.1@usc.edu).

Lauren H. Smith is with the Center for Bionic Medicine at the Rehabilitation Institute of Chicago and the Department of Physical Medicine and Rehabilitation, Northwestern University, Chicago, IL, USA, 60611 (Phone: +312-238-2084, Email: lauren-smith@fsm.northwestern.edu).

Levi J. Hargrove is with the Center for Bionic Medicine at the Rehabilitation Institute of Chicago and the Department of Physical Medicine and Rehabilitation, Northwestern University, Chicago, IL, USA, 60611 (Phone: +312-238-2084, Email: l-hargrove@northwestern.edu).

Douglas J. Weber is with the Department of Physical Medicine and Rehabilitation, University of Pittsburgh, Pittsburgh, PA USA 15260 (Phone: +412-624-4055, Email: djw50@pitt.edu).

Gerald E. Loeb is with the Department of Biomedical Engineering, University of Southern California, Los Angeles, CA USA 90089 (Phone: +213-821-5311, Email: gloeb@usc.edu).

nerve. The axonal conduction velocity was measured from the femoral nerve cuff records. For 43 out of these 51 MNs, the corresponding target muscle was identified by spike-triggered averaging of signals recorded from bipolar EMG electrodes implanted in one of the anterior thigh muscles: vastusintermedius, medialis and lateralis, sartorius anterior and medialis, and rectus femoris. With 10-12 electrodes in the ventral roots, the number of discriminable MUs on a given day was rarely more than five and the amplitude of their action potentials was uncorrelated with their conduction velocity or recruitment order.

Targeted Muscle Reinnervation (TMR) is a surgical technique that transfers residual arm nerves to alternative targeted muscle sites following amputation of their originally innervated muscles [8, 9, 10, 11, 12]. After reinnervation, these target muscles produce electromyogram (EMG) signals that are much larger and more easily recorded than the action potentials from the motoneurons. This technique has been applied to several high-level amputees and allowed for much better control using surface EMG signals in comparison to using other control options [9].

The EMG signals recorded transcutaneously or intramuscularly from the TMR muscle are likely to consist of small numbers of discriminable single MUs whose amplitude may not accurately reflect their relative MN size or recruitment order. This is because the reinnervation process results in clumps of muscle fibers innervated by a single motor axon rather than the highly intermingled matrix of many motor units found in normally innervated muscles [13]. Simply rectifying and integrating the electrical signals of MUs (as is done with gross EMG from intact muscles [2]) may not produce an accurate estimate of MNP excitation if the amplitude of the constituent MUs is not correlated with their order of recruitment. This is particularly true if only a small number of MUs are contributing to the recorded signal. Thus, the challenge is to develop an algorithm that can make the best possible estimate of MNP excitation from the recruitment and firing rates of a small number (2-10) of discriminable MUs.

II. Algorithm Design

The firing frequency of early recruited MUs correlates well with onset of the simultaneously recorded EMG signals from the whole intact muscle in animals, which, in turn, reflects the excitation of the whole MNP. The later recruited MUs generally start firing when the excitation reaches a specific threshold level. Their frequency is then modulated according to the time course of the excitation amplitude above this threshold, which can be measured from the EMG signals [13, 14]. There tends to be a common initial firing frequency for MUs of a given type, and their firing frequencies converge to a single maximal firing frequency at maximal activation [15]. There is a suggestion that the frequency modulation of earlier recruited units is hyperbolic rather than linear [16, 17].

We used these properties to design a novel estimation scheme for the MNP activation over the entire range of recruitment from the sparse recordings from the ventral root or TMR muscles in amputees. The algorithm is called Sparse Optimal Motor Estimation (SOME). It works by mapping the instantaneous firing rate of each recorded MU into the excitation level that tends to cause that MU activity. The $SOME$ algorithm predicts a total excitation level for the MNP, which can be fed into a model of the limb to estimate actual muscle force output and the resulting kinematics.

A. Sampling of Motoneuron Pool

We first define the parameters for a MNP recruitment model with a set of N discriminable MUs, $\mathcal{S} = \{MU_1, ..., MU_i, ..., MU_N\}$, $1 \leq i \leq N$. The MNP recruitment model is fully defined when all N MUs are available and the dimensionality of the MNP set $|\mathcal{S}_{full}| = N$. The relationship between the net excitatory drive and firing rate for each MU_i was defined as $f_i(u)$, $i = 0, 1, 2, ..., N$. For each motor unit MU_i, $r_i^k = 1/(s_i^k - s_i^{k-1})$ is the instantaneous firing rate of k^{th} spike at the spike timing s_i^k. It is also a function of the excitation input at the sampled spike timing, which is defined as $r_i^k = f_i[u(s_i^k)]$. The challenging problem is how to reconstruct the net excitatory drive from a sparse sampling of the entire MNP, which has a much smaller number of discriminable MUs $|\mathcal{S}_{full}| \ll N$.

In order to bracket the possibilities of different modulation patterns of MUs [18], we created and tested three different simulations: saturation recruitment model, continuous modulation model and "onion skin" recruitment model, each with 5 slow MUs (labeled $MU_1 - MU_5$) and 5 fast MUs (labeled $MU_6 - MU_{10}$). For a MNP of 10 MUs with equal probability to be recorded, the possible combinations of the MNP sampling can be calculated by using the binomial coefficient formula,

$$\left(\begin{array}{c} N \\ n \end{array} \right) = \frac{N!}{n!(N-n)!} \tag{1}$$

as 1, 10, 45, 120, 210, 252, 210, 120, 45, 10, and 1 corresponding to the number of MUs $n = 0, 1, 2, ..., 10$. More general case of partial samplings are the number of MUs falls in $2 \leq n \leq 9$.

In order to better demonstrate the sparse sampling of the MNP, we generated the sparse matrix $C^n(i, j)$ and display as image (Fig.2), where the row index $i = 1, 2, ..., 10$ corresponds to the MU ID number, and the column index is a realization of the combination with selected number of n MUs. When $C^n(i, j) = 1$, with corresponding blacksquare in the image indicate for the occurrence of certain MU, whereas value 0 indicates null detection. The matrix C^n is a sparse matrix populated primarily with zeros when there is no measure value for a particular MU. Figure 5 illustrates nine matrices C^n with $n = 1, 2, ..., 9$. This extensive repertoire of sampling combination provides a more realistic behavior space for systematic exploration of algorithm accuracy as a function of the number of MUs.

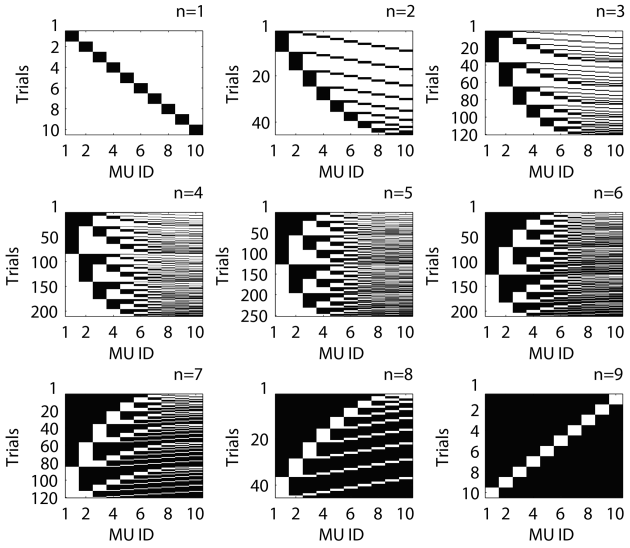

Figure 2. Illustration of possible sparse sampling combinations for different number of MU from a MNP of 10 MUs. Black box indicates the selection of the particular MU with number ID label in the x-axis. White color means no record of information for the corresponding numbered MU.

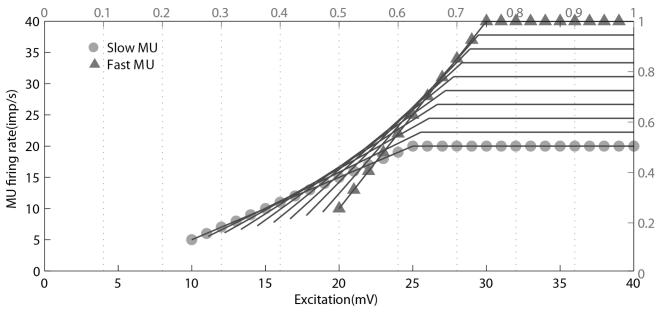

Figure 3. The excitation and firing relationship of the Saturating Recruitment Model for a MNP of 10 MUs . The sparse sampling of the MNP contains only two MUs: slow (solid dot) and fast (solid triangle). As the net excitation to the MNP increases, slow starts firing at $5\,imp/s$ and saturates at $20\,imp/s$. The fast starts firing at $10\,imp/s$ at a higher level of excitation and saturates at $40\,imp/s$. The excitation to the MNP is normalized from 0 to 1 (scale in the top) and MU firing rate is also scaled on the right.

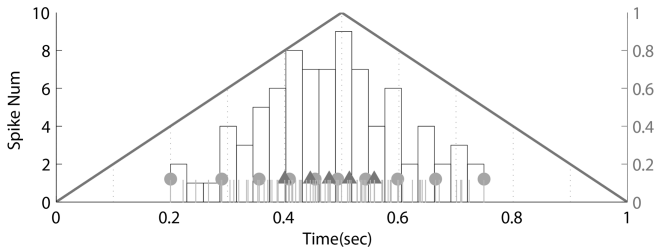

Figure 4. The spikes of 10 MUs in the entire motor neuron pool (vertical gray bin). The spikes of slow MU is labeled with solid dot while the fast MU is marked with solid triangle. The histogram distribution (unfilled bar) is plotted for the spike timing with bin size of $50\,ms$ under the normalized excitation input (scale on the right) with a symmetric ramp (solid line).

B. Sparse Optimal Motor Estimation Algorithm

We first apply the saturating recruitment model to derive the algorithm, in which the sparse MNP model has only two MUs: MU_1 (the first recruited slow unit) and MU_{10} (the last recruited fast unit). Their firing rates over the full range of net excitatory drive to the MNP were simulated according to the relationship shown in Figure 3. In the example provided here, the MU_1 starts to fire at $5\,imp/s$ when excitation reaches $10\,mV$, and the firing rate saturates at the $20\,imp/s$ when the excitation input is $25\,mV$ and above. The MU_{10} starts to fire at $10\,imp/s$ when excitation reaches $20\,mV$ and plateaus at a peak firing rate of $40\,imp/s$ when the excitation exceeds $30\,mV$. The firing rate ranges are based on the default values in Virtual Muscle [19], which normalizes firing rates according to $f_{0.5}$, the firing frequency that produces half the maximal tetanic force for each MU ($10\,imp/s$ for slow MU_1, $20\,imp/s$ for fast MU_{10}). A tendency for firing rate to saturate at high force output can be seen in some experimental records (as discussed for similar ramps in [14]) and is inherent in the after-hyperpolarization mechanism of the α-MNs [20, 21].

A symmetric triangular ramp was used as the excitation input approximating similar physiological experiments [22, 23] and simulated spike occurrences for the two MUs are depicted in Figure 4. The histogram distribution (unfilled bar) is plotted for the spike timing with bin size of $50ms$ under the normalized excitation input (scale on the right). The aggregate activity of the asynchronous units is very noisy, even when integrated into $50\,ms$ bins typical for updating command signals to prosthetic systems.

As a consequence of the interaction between having both an increased recruitment of MUs and an increase in the asynchronous firing frequency of MU with increasing excitation, the relationship between excitation and the cumulative spike rate from all MUs becomes very nonlinear. The question is how to combine the information from a small number of all MUs firing asynchronously at rates that are modulated smoothly. The frequent occurrence of individual MU spikes provides an opportunity to implement much more frequent and less noisy estimates of MNP excitation, which is exploited by the $SOME$ algorithm.

This estimation algorithm employs different strategy for rising ramp and falling ramp. If the excitation is increasing as determined by comparing firing rates at previous and current time steps (line 5), the excitation estimate is updated on the occurrence of each successive MU spike (line 6-8). If the excitation is decreasing as determined by line 9, when a spike is expected given the previous excitation level and the time elapsed since the last spike for all MUs (line 10), the absence of a spike that is "due" to occur given the previous interval can be used to estimate the maximal level of excitation that is consistent with the absence of spikes. If no spikes occur in any MUs, then the excitation estimate falls rapidly from one exponential to another according to the lowest trajectory and updates as exponential decay (line 11-12) where γ is the arbitrary decreasing rate between 0 and 1 (0.8 in this paper).

Sparse Optimal Motor Estimation Algorithm

Input: Observed MUAPs $\underline{s} = \begin{bmatrix} t_0 & t_1 & \cdots & t_j & \cdots & t_m \end{bmatrix}$
Input: Calibrated function $f_i(u)$ for observed MU_i
Output: Estimated excitation $\hat{u}(t)$

START
$\hat{u}(t) = 0$ **for** $t = [0, t_0)$
$\hat{u}(t_0) = \min\{\epsilon_i, \forall i\}$
  WHILE $|\underline{s}| \neq 0$
    IF $f_i[\hat{u}(t_{j-1})] \leq 1/(t_j - t_{j-1})\ \exists i$
      $u(s_i^k) = \max\{f_i^{-1}(\frac{1}{t_j - t_{j-1}}),\ \forall i\}$
      $\hat{u}(t) = u(s_i^k)$ **for** $t = [t_{j-1}, t_j]$
      $j = j++$
    IF $f_i[\hat{u}(t_{j-1})] > \frac{1}{t_j - t_{j-1}}\ \forall i$
      $\hat{u}(t) = u(s_i^{k-1})$ **for** $t = [t_{j-1}, t_{j-1} + \frac{1}{r_i^{k-1}}]$
      $\hat{u}(t) = u(s_i^{k-1}) e^{-\gamma(t - t_{j-1} - \frac{1}{r_i^{k-1}})}$
      for $t = [t_{j-1} + \frac{1}{r_i^{k-1}}, t_j]$
      $j = j++$
  END WHILE
END

The output of the $SOME$ algorithm is illustrated by the gray solid trace in Figure 5. For comparison, the true excitatory input is plotted in red ramp trace and the actual spike occurrences are labeled by dots and triangle with sequential number). As excitation increases ($0 \leq t \leq 0.5$), the first spike (#1) and subsequent spikes (#2-9) timing provides successively higher and momentarily accurate estimates of the total excitation drive. As excitation decreases ($0.5 \leq t \leq 1$), the estimates start to drop as individual spikes that were "due" to occur (e.g., spike #14) given the previous (e.g., spike #13) estimate fail to occur.

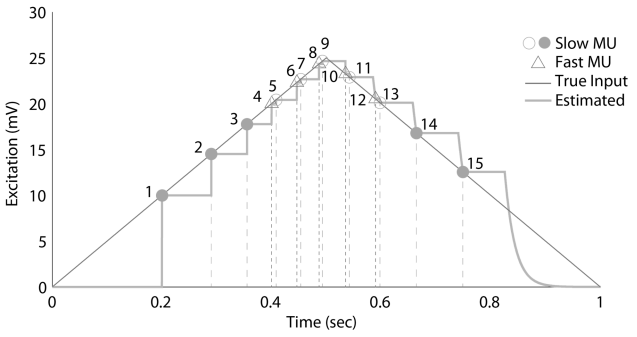

Figure 5. Estimated excitation input (gray solid line) based on the MUAPs from the slow MU (dot) and fast MU (triangle) using proposed $SOME$ algorithm. True excitation input is depicted in solid line and each spike event is numbered in the order of appearance.

The interval between individual Motor Unit Action Potential (MUAP) is fairly long (100 to 200 ms for 10 to 5 imp/s, respectively) compared to the rate at which the excitation signal to the MNP may actually be modulated. Waiting for the next spike in a given train or aggregating the asynchronous events and taking a running average tends to be slow and/or noisy; therefore it is imperative to derive as much information as possible from the timing of each spike in MUAP trains.

C. Simulation on Different Recruitment Patterns

We then simulated the $SOME$ algorithm on two different recruitment patterns. In the Continuous Modulation Model (Fig.6 left) [19], the MUs also have type-specific ranges of firing rates and continuously graded recruitment thresholds, but all MUs reach their maximal firing rates only at maximal excitation. In the "Onion Skin" Recruitment Model (Fig.6 right), all MUs have the same range of firing rates from $10 - 40 imp/s$ and reach the maximal rate together at maximal excitation. This is consistent with single MU recordings in which the firing rates of MUs during force-varying contractions have a hierarchical organization like an "onion skin", in which the early recruited units are always firing at a higher frequency than later recruited MUs [24, 25, 26]. It has been hypothesized that this phenomenon is the result of the hierarchical response of individual MUs to a "common drive" of the MNP from supraspinal motor centers [24], but it may simply reflect the technical difficulty of obtaining reliable single MU behaviors at high muscle force levels.

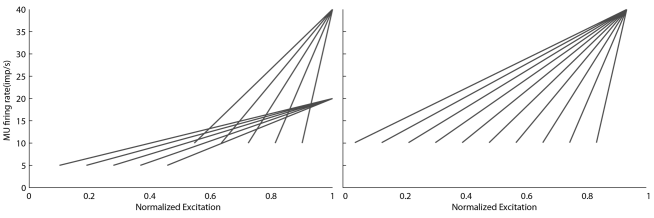

Figure 6. The continuous modulation (left) and "Onion Skin" recruitment model (right) with 10 motor units (5 slow MUs and 5 fast MUs). Each MU has its own pre-defined threshold, and the firing rates have been normalized to . For continuous modulation mode, is $10 imp/s$ for the slow MUs and $20 imp/s$ for the fast MUs. For "Onion Skin" recruitment model is $10 imp/s$ for both the slow and fast MUs.

All of the models assumed that the last recruited MU did not start firing until 80-90% of maximal excitatory drive. This is a conservative value because muscles in which all MUs are recruited at lower drives will provide fewer combinations of sparse sampling for which some of the MUs are not active at all. A normalized ramp excitation $u(t)$ was simulated with maximum input of one and duration of one second. As $u(t)$ increases, more MUs are recruited until all of them are recruited, and continuing increases in excitation result only in frequency modulation of MUs. It appears that both slow and fast MUs have the same minimum firing frequency range $[f_{min},\ f_{max}]$, in the units of $f_{0.5}$, which is the frequency that produces the half of the maximal isometric muscle force. The normalize frequency $f_{0.5}$ has different values depending on MU type, and all MUs finally reach the normalized peak firing rate $2 f_{0.5}$ at maximum excitation. The recruitment threshold of a given MU is determined based on a

combination of the cumulative fractional Physiologic Cross-Sectional Area (PCSA) of all prior recruited MUs. This is the recruitment scheme incorporated into the Virtual Muscle software package [19] [1]. In this Continuous Modulation model we chose $f_{0.5} = 10\,imp/s$ for slow MU ($f_{min} = 5$, $f_{max} = 20$) and $f_{0.5} = 20\,imp/s$ for fast MU ($f_{min} = 10$, $f_{max} = 40$), which are the same ranges as saturating model. The Onion Skin Recruitment model is simulated in this section, which is similar to the Continuous Modulation model but the range of firing rates for all MUs, both fast and slow, covering the same range of $10 - 40\,imp/s$, as shown in Figure 6 (right). This was actually accomplished in Virtual Muscle by changing the firing range of the slow MUs to $f_{min} = f_{0.5}$, $f_{max} = 4f_{0.5}$ rather than changing , which determines various aspects of force production.

The $SOME$ algorithm is designed to provide the best possible estimate of MNP excitation regardless of the number of MUs actually recorded, but the performance of the sparse estimation algorithm depends on the sparse sampling combination as well as the characteristics of each MU, which is analyzed in the following sensitivity studies for different recruitment patterns. We simulate all the sparse sampling scenarios of a MNP with 10 MUs. Figure 7 shows the corresponding MUAPs (indicated by tick marks) for all the possible combinations of 10 MUs from continuous modulation model (see corresponding Fig.5) in response to the ramped up and down excitatory drive.

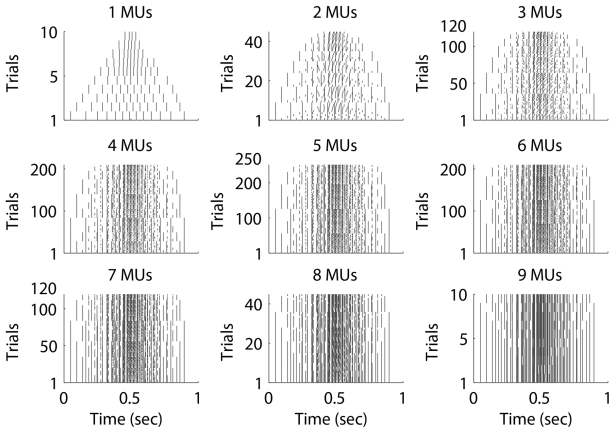

Figure 7. Raster plot of the MUAPs (vertical tick marks) for every possible combination of various numbers of MUs in the MNP of continuous modulation model (as illustrated in Fig.5). All simulations used the same excitation ramp. Same analysis is performed for "Onion Skin" model.

We use $\frac{1}{N}\sum_{i=1}^{N}(\hat{u}_i - u_i)^2$, the mean value of the squared deviations of the predictions from the true values, to compute the Mean Square Error (MSE) for every single trial in each combination subset, and then applied boxplot to analyze the statistic distribution of the combination superset. For the worst scenario, when there is no detection of any MU (the dimension of the subset is zero), the MSE of the estimation becomes $\mathrm{MSE}(\hat{u}) = \frac{1}{N}\sum_{i=1}^{N} u_i^2$. The maximum estimation error for the simulated ramp excitation input is $\frac{1}{N}\sum_{i=1}^{N} u_i^2 = 0.5$, which is in fact the entire area under the excitation input curve. To better demonstrate the variation of the estimation error, we used the normalized MSE,

$$\overline{\mathrm{MSE}}(\hat{u}_i) = \frac{1}{N}\frac{\sum_{i=1}^{N}(\hat{u}_i - u_i)^2}{\sum_{i=1}^{N} u_i^2}. \qquad (2)$$

and plotted all the boxplots in logarithm scale of base 10 as $log_{10}[\overline{\mathrm{MSE}}(\hat{u}_i)]$. The estimation errors for different numbers of MUs were analyzed in the boxplot of Figure 8.

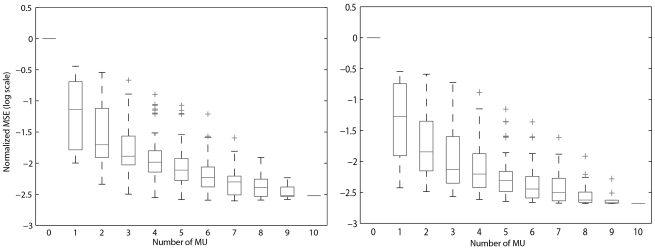

Figure 8. Box plot of the mean squared error (MSE; log scale) of predicted excitation for continuous modulation (left) and "Onion Skin" recruitment model (right). Number of MUs sampled by the $SOME$ algorithm ranges from 0 to 10; each box shows the range of estimates from all the possible combinations of MUs; the central red line is the median, the edges of the box are the 25th and 75th percentiles, the whiskers denote ±2.7 std. dev., outliers denoted by crosses.

As Figure 8 indicates, the maximum MSE is $log_{10}1 = 0$ and it decreases rapidly with increasing the number of MUs available for estimation. The logarithm scale provides a fractional quantification, where "-1" means 0.1 or 10% maximum error and "-2" means 0.01 or 1% maximum error, etc. The scatter depends on the existence of sampled subsets that are disadvantageous, particularly those only composed of the late-recruited, fast MUs that provide no information during the early and late stages of the ramp excitation when they are not firing at all (see outlier data points marked as red crosses in Fig.8). The majority error for the single MU estimation cases arises from the portions of the ramp during which no MU recording is available, which is largest for the fastest MUs. When all 10 MUs are available, the $SOME$ algorithm captures the ramp excitation quite well and the error is very small. There are also some unusually good predictions that correspond to fortuitous combinations of unit types and individual spike timings that provide more steady updates of the estimated excitation. The estimation result indicates that the designed algorithm is robust to different MNP models. In fact, performance for "Onion Skin" recruitment model is slightly better because the higher spike rates provide more frequent estimates of excitation level.

III. Validation with Experimental Data

The idealized simulations above assume noise-free recruitment and perfect discrimination of MUs. Real MU activity necessarily includes the effects of synaptic and membrane

[1] available from http://mddf.usc.edu

noise and its interaction with slowly fluctuating cellular processes such as after-hyperpolarization [27, 28]. The discrimination and identification of individual spikes from each MU is unlikely to be perfect. Some degree of smoothing may be necessary to obtain a reliable control signal from the $SOME$ algorithm without compromising its ability to follow rapid changes in MNP excitation. The following analysis of actual MU activity provides a more realistic assessment of the performance of the $SOME$ algorithm compared to simple rectification and integration of available gross EMG signals.

In order to use the $SOME$ algorithm with an amputee, it is necessary to calibrate the threshold and frequency modulation of each available MU in terms of the intended excitation to each MNP. In validation experiments using intact human or animal subjects, the gross EMG from the parent muscle is available for calibration, but no such signal is available from an amputee. Instead, it will be crucial to instruct subjects to perform a set of virtual movements with systematic ramping of effort to associate the MU activity with a particular muscle function. In the case of muscles operating on multiple degrees of freedom in the skeletal system, the imputed membership in a MNP will have to be extracted based on statistical correlations with multiple virtual movements that would normally require different combinations of muscle activation, which remain to be developed.

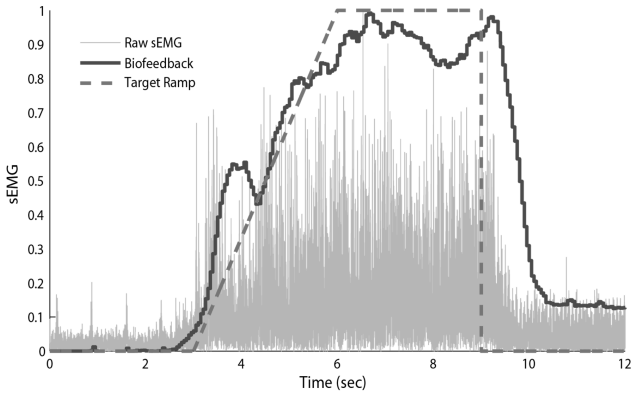

Figure 9. Raw surface EMG signal recorded from the experiment of tracking the "virtual ramp of effort" (dash red line), and reconstructed biofeedback signal (solid blue line).

The intramuscular EMG signals available from TMR muscles were evaluated according to the following experimental protocol that was approved by the Northwestern University IRB. One male shoulder disarticulated amputee who had undergone TMR surgery approximately 10 years previously for the purposes of improving the control over a commercially available powered prosthesis participated in this experiment.The subject tracked a "virtual ramp of effort" of elbow extension (Fig.9) by matching the integrated and heavily smoothed ($750\,ms$ moving average labeled Biofeedback) surface EMG (sEMG) to a slowly rising visual ramp up to what the subject perceived was his/her maximal voluntary contraction (MVC). Both the intramuscular and surface EMG were recorded from the TMR patient's "hand closed" site (median nerve reinnervation), "elbow down" site (radial nerve reinnervation), and"elbow up" site (musculocutaneous nerve reinnervation). All of these control sites were part of the patient's reinnervatedpectoralis muscle. The $SOME$ algorithm utilizes the EMG signal recorded from the "elbow up" site muscleto derive the patient's control command.

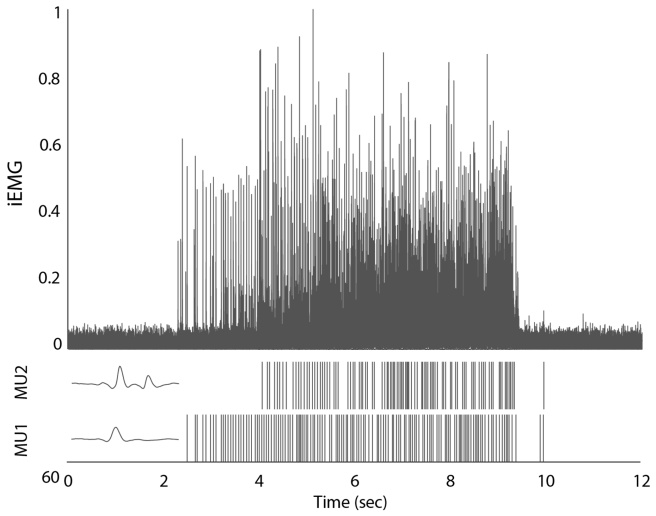

Figure 10. Raw intramuscular EMG signal and extracted spike time (MU1 and MU2) and unit waveforms ($20\,ms$ duration inserts) during ramp effort quantified by Fig.9.

The intramuscular EMG (iEMG) signals were recorded from bipolar fine wire electrodes (CareFusion) using a 10-channel Motion Lab Systems MA300 system with x4000 gain and sampled at $10\,kHz$ by a National Instruments USB-6218 DAQ. The signal was bandpass filtered between $20\,Hz$ and $2\,kHz$. The surface EMG signals were recorded from the Delsys Bagnoli Desktop System with x1000 gain and sampled at $1\,kHz$. The sEMG is bandpass filtered between $20\,Hz$ and $450\,Hz$. Both the iEMG and sEMG signals were rectified, filtered and normalized to the MVC level. Two MU firing patterns (Fig.10) were manually discriminated from the iEMG signal according to their distinctive waveforms (inserts in Fig.10) during a voluntary ramp up to MVC. The instantaneous firing rates of two MUs are computed from their MUAP time (Fig.11 top). Their instantaneous firing rates were calibrated to excitatory drive as estimated from the normalizedsEMG (Fig.11 bottom). The $SOME$ algorithm was used to estimate MNP excitation during the ramp effort (thick gray solid traces in Fig.12) for comparison to the rectified and bin-averaged sEMG and iEMG signals with similar bin durations.

The $SOME$ algorithm captures many detailed features of the sEMG envelope, including some of the rapid features of sEMG modulation that are apparent with the shorter bin durations of 20 and $50ms$. The $SOME$ output remains at zero until the first MU is recruited and then reflects the rapid onset and overshoot of the recruitment that the subject

attempts to correct around the 4s mark when very slow biofeedback signal was visualized. The rectified output of the iEMG channel from which the MUs were discriminated reflects less well the trends in the sEMG, which provides the best available estimate of excitation under these unstable conditions of recruitment with delayed visual feedback.The iEMG signal suffers from being dominated by the two large MUs firing at relatively low rates compared to the smoothing bins, resulting in stochastic fluctuations unrelated to MNP excitation.

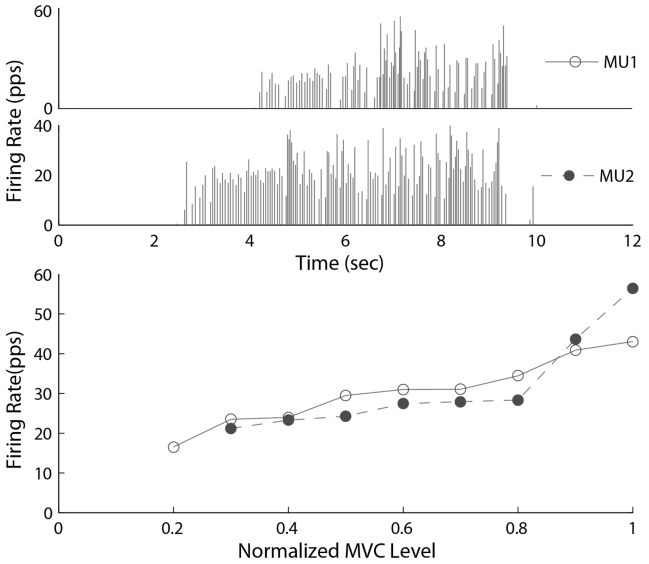

Figure 11. The instantaneous firing rates of two MUs (in pulses per second vs. time, top) and as a calibration function of normalized sEMG amplitude from Fig.9 (bottom).

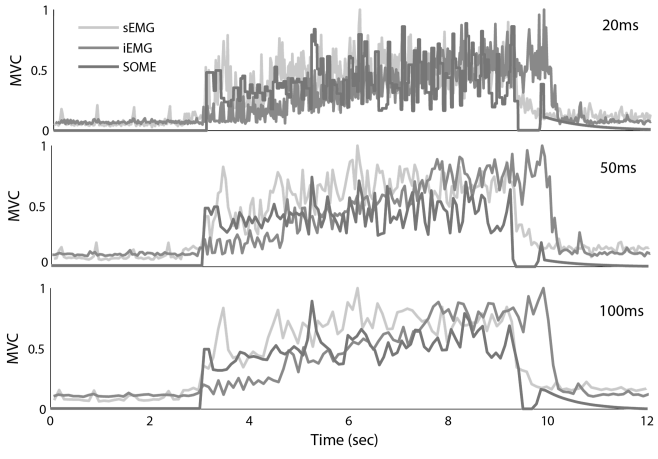

Figure 12. Comparison of $SOME$ algorithm output (red trace) to rectified sEMG (light gray trace) and iEMG (dark gray trace). Bin-averaged results are compared for bin durations of $20\,ms$, $50\,ms$, and $100\,ms$ applied to the output of the $SOME$ algorithm as well as the rectified EMGs.

IV. Discussion and Future Work

We have validated the $SOME$ algorithm on the EMG data recorded from a shoulder disarticulated amputee with targeted motor reinnervation surgery. The relatively long and complex unit signatures obtained from these TMR muscles (e.g. MU2 in Fig.5) may be a feature of the reinnervation process and will make it particularly difficult to obtain suitable spike discrimination when multiple units are active because of their tendency to overlap and occlude each other. The future evaluation of $SOME$ algorithm will be performed on ventral root and peripheral nerve recordings, where the unit waveforms tend to be much briefer and there is less background activity [3].

The TMR validation experiment serves to demonstrate the functionality of the $SOME$ algorithm with noisy MU firing patterns. It remains to be tested using novel data sets apart from those used to calibrate the MU firing rates. Such tests would preferably include more rapid fluctuations of effort, which will take advantage of the algorithm's ability to estimate excitation without the delays inherent in smoothing functions. The $SOME$ algorithm is particularly useful to estimate rapidly changing patterns of MNP recruitment such as associated with quick, phasic movements, when long integration times or filter delays are undesirable for control signals. The recruitment and firing rates of MUs appear to be influenced by the slope of such ramps as well as absolute level of motor drive [14], so it will be important to calibrate the $SOME$ algorithm for more rapid ramps.

The use of the $SOME$ algorithm assumes that there are no false positives or false negatives in the MU spike discrimination. The incidence of such errors will vary greatly with the method and quality of the recordings. A missed spike in a single MU train will result in an instantaneous drop of the perceived rate. Such an error would be rapidly corrected if other MUs were contributing but could result in a substantial underestimate if only the one MU was active. Extra spikes such as misclassification of another MU can result in unphysiologically high perceived firing rates, which will need to be capped by other refinements to the algorithm. Both types of error presumably contribute to some of the larger fluctuations in instantaneous firing rate apparent in Figure 11 (top). Because actual muscle recruitment tends to change smoothly during voluntary activity such as controlling prosthesis, a $Kalman$ filter could be used to improve performance, but that is outside the scope of this study.

In order to use the $SOME$ algorithm with an amputee, it is necessary to calibrate the threshold and frequency modulation of each available MU terms of the intended excitation to each MNP. In validation experiments using intact human or animal subjects, the gross EMG from the parent muscle is available for calibration, but no such signal is available from an amputee.Instead, it will be crucial to instruct subjects to perform a set of virtual movements with systematic ramping of effort to associate the MU activity with a particular muscle function. For rapidly modulated ramps, it will probably be better to use the subject's own imagined ramp or an acoustic cue without feedback in order to avoid the substantial delay in visual feedback, which appeared to result in stepwise

corrections rather than the desired smooth modulations in MNP excitation and recruitment.

Eventually, a proper designed prosthetic device with fast dynamic response will be incorporated in the experiments to test whether $SOME$ output is accurate and useful for control when different types of signal processing are compared in a complete control loop. In the case of muscles operating on multiple degrees of freedom in the skeletal system, the imputed membership in a MNP will have to be extracted based on statistical correlations with multiple virtual movements that would normally require different combinations of muscle activation, which remain to be developed with the help of neuromusculoskeletal modeling software [29,30].

ACKNOWLEDGMENT

This research is funded by DARPA/SPAWAR, Contract No. N66001-11-C4141, titled: Reliable Spinal Nerve Interfaces for Sensorimotor Neuroprotheses, and Howard Hughes Medical Institute Medical Research Fellows Program.

REFERENCES

[1] Henneman, E. and Mendell, L. M., "Functional organization of the motoneuron pool and its inputs," in Handbook of Physiology. Sect. I. The Nervous System. Vol II, Part 1, V. B. Brooks, Ed., ed Washington, DC: American Physiological Society, 1981, pp. 423-507.

[2] Loeb, G. E. and Gans, C., Electromyography for experimentalists. University Chicago Press, 1986, pp. 38

[3] Hoffer, J. A., Sugano, N., Loeb, G. E., Marks, W. B., O'Donovan, M. J., and Pratt, C. A., "Cat hindlimbmotoneurons during locomotion. II. Normal activity patterns," J.Neurophysiol., vol. 57, pp. 530-553, 1987.

[4] Hoffer, J. A., O'Donovan, M. J., Pratt, C. A., and Loeb, G. E., "Discharge patterns in hindlimbmotoneurons during normal cat locomotion," Science, vol. 213, pp. 466-468, 1981.

[5] Branner, A., Stein, R. B., Fernandez, E., Aoyagi, Y., and Normann, R. A., "Long-term stimulation and recording with a penetrating microelectrode array in cat sciatic nerve," IEEE Trans on Biomedical Engineering, vol. 51, pp. 146-157, 2004.

[6] Juan Ordonez, Martin Schuettler, Christian Boehler, Tim Boretius and Thomas Stieglitz (2012). "Thin films and microelectrode arrays for neuroprosthetics." MRS Bulletin, 37 , pp 590-598

[7] Farina, D.; Negro, F." Accessing the neural drive to muscle and translation to neurorehabilitation technologies," Biomedical Engineering, IEEE Reviews in , vol.PP, no.99, pp.1-14

[8] Hoffer, J.A., and Loeb, G.E. "Implantable electrical and mechanical interfaces with nerve and muscle," Ann. Biomed. Engng., vol. 8, pp. 351-360, 1980.

[9] Kuiken T. Targeted reinnervation for improved prosthetic function. Phys Med RehabilClin N Am. 2006 Feb;17(1):1-13.

[10] Kuiken, T. A., Dumanian, G. A., Lipschutz, R. D., Miller, L. A., and Stubblefield, K. A., "The use of targeted muscle reinnervation for improved myoelectric prosthesis control in a bilateral shoulder disarticulation amputee," Prosthet.Orthot.Int., vol. 28, pp. 245-253, 2004.

[11] Kuiken TA, Miller LA, Lipschutz RD, Lock B, Stubblefield K, Marasco P, Zhou P, Dumanian G. "Targeted reinnervation for enhanced prosthetic arm function in a woman with a proximal amputation". Lancet 369: 371–380, 2007.

[12] P Zhou, M M. Lowery, K B. Englehart, H Huang, G Li, L Hargrove, J P. A. Dewald and Todd A. Kuiken, "Decoding a New Neural-Machine Interface for Control of Artificial Limbs" J Neurophysiol 98:2974-2982, 2007.

[13] Borg, J., Grimby, L., and Hannerz, J., "Axonal conduction velocity and voluntary discharge properties of individual short toe extensor motor units in man," The Journal of Physiology, vol. 277, pp. 143-152, 1978.

[14] Milner-Brown, H. S., Stein, R. B., and Yemm, R., "The orderly recruitment of human motor units during voluntary isometric contractions," Journal of Physiology, vol. 230, pp. 359-370, 1973.

[15] De Luca, C. J., Foley, P. J., and Erim, Z., "Motor unit control properties in constant-force isometric contractions," Journal of Neurophysiology, vol. 76, pp. 1503-1516, 1996.

[16] Anna M. Taylor,Evangelos A. Christou, and Roger M. Enoka "Multiple Features of Motor-Unit Activity Influence Force Fluctuations During Isometric Contractions" JN Physiol August 1, 2003 vol. 90 no. 2 1350-1361

[17] Monster, A. W. and Chan, H., "Isometric force production by motor units of extensor digitorumcommunis muscle in man," Journal of Neurophysiology, vol. 40, pp. 1432-1443, 1977.

[18] Fuglevand, A. J., Winter, D. A., and Patla, A. E., "Models of recruitment and rate coding organization in motor-unit pools," J.Neurophysiol, vol. 70, pp. 2470-2488, 1993.

[19] Cheng, E., Brown, I. E., and Loeb, G. E., "Virtual Muscle: A computational approach to understanding the effects of muscle properties on motor control," J.Neurosce.Methods, vol. 101, pp. 117-130, 2000.

[20] Baldissera, F. Gustafsson. B. "Firing behavior of a neuron model based on the afterhyperpolarization conductance time course and algebraical summation." Adaptation and steady state firing. Actaphysiologicascandinavica 92,27-47. 1974

[21] Baldissera, F., Gustafsson, B. and Parmiggiani, F. "Saturation summation of the afterhyperpolarization conductance in spinal motoneurones: a mechanism for 'secondary range' repetitive firing". Brain Research 146, 69-82. 1978

[22] Kato, M., Murakami, S., and Yasuda, K., "Behavior of single motor units of human tibialis anterior muscle during voluntary shortening contraction under constant load torque," Experimental Neurology, vol. 90, pp. 238-253, 1985.

[23] Bawa, P., Chalmers, G. R., Jones, K. E., Søgaard, K., and Walsh, M. L., "Control of the wrist joint in humans," European Journal of Applied Physiology, vol. 83, pp. 116-127, 2000.

[24] De Luca, C. J., LeFever, R. S., McCue, M. P., and Xenakis, A. P., "Behavior of human motor units in different muscles during linearly varying contractions," Journal of Physiology, vol. 329, pp. 113-128, 1982.

[25] De Luca, C. J. and Erim, Z., "Common drive of motor units of regulation of muscle force," Trends in Neurosciences, vol. 17, pp. 229-305, 1994.

[26] Westgaard, R. H. and De Luca, C. J., "Motor Control of Low-Threshold Motor Units in the Human Trapezius Muscle," Journal of Neurophysiology, vol. 85, pp. 1777-1781, 2001.

[27] Matthews PB. "Relationship of firing intervals of human motor units to the trajectory of post-spike after-hyperpolarization and synaptic noise". J Physiol 492:597–628, 1996

[28] [28] S Andreassen and A Rosenfalck, "Regulation of the firing pattern of single motor units."JNeurolNeurosurg Psychiatry. 1980 October; 43(10): 897–906.

[29] [29] Hauschild, M., Davoodi, R., and Loeb, G. E., "A virtual reality environment for designing and fitting neural prosthetic limbs," IEEE Trans Neural Syst.RehabilEng, vol. 15, pp. 1-7, 2007.

[30] Delp, S. L. and Loan, J. P., "A graphics-based software system to develop and analyze models of musculoskeletal structures," Computers in Biology and Medicine, vol. 25, pp. 21-34, 1995.

Yao Li received the B.S. degree in electrical engineering from Sichuan University, Chengdu, China in 2002 and Ph.D. degree in electrical and computer engineering, from the University of Maryland, College Park in 2010. Since then, he has been working as a research associate at the University of Southern California. He is mainly interested in the application of control theory and modeling of complex systems to the understanding and treatment of human sensorimotor disorders. He was a visiting scholar at the National Center for Simulation in Rehabilitation Research (NCSRR) at Stanford University in 2011. He is interested in developing the optimal estimation algorithms for deriving command signals for prosthetic limbs from the residual peripheral nervous system of amputees. He is also interested in the development and experimental validation of models of sensorimotor learning that have important clinical implications and robotic applications of a robust tactile sensor array that mimics the mechanical properties and distributed touch receptors of the human fingertip.

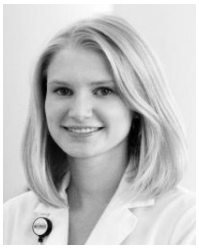

Lauren H. Smith received the B.S. degree in biomedical engineering in 2008 from Northwestern University, Evanston, IL, USA. She is currently pursuing both the M.D. degree and the Ph.D. degree in biomedical engineering at Northwestern University, Chicago, IL, USA. Her research interests include neural interface, bioelectric signal analysis, and clinical neurophysiology.

Levi J. Hargrove (S'05 - M'08) received his B.Sc. and M.Sc. and PhD degrees in electrical engineering from the University of New Brunswick (UNB), Fredericton, NB, Canada, in 2003 2005, and 2007 respectively. He joined the Center for Bionic Medicine at the Rehabilitation Institute of Chicago in 2008. His research interests include pattern recognition, biological signal processing, and myoelectric control of powered prostheses. Dr. Hargrove is a member of the Association of Professional Engineers and Geoscientists of New Brunswick. He is also a Research Assistant Professor in the Department of Physical Medicine and Rehabilitation (PM&R) and Biomedical Engineering, Northwestern University. Evanston, IL, USA.

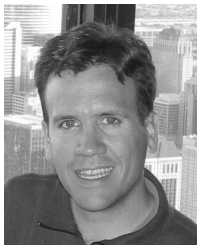

Douglas J. Weber received a B.S. ('94) in Biomedical Engineering from the Milwaukee School of Engineering and an M.S. ('00) and Ph.D. ('01) in Bioengineering from Arizona State University. He was a postdoctoral fellow ('01-03') and Assistant Professor ('03-'05) in the Center for Neuroscience at the University of Alberta before joining the University of Pittsburgh. He is an Associate Professor in the Department of Bioengineering at the University of Pittsburgh and a Research Biomedical Engineer at the Department of Veteran's Affairs. He is also a faculty member in the Department of Physical Medicine and Rehabilitation and the Center for the Neural Basis of Cognition. His primary research area is Neural Engineering, including studies of motor learning and control of walking and reaching with particular emphasis on applications to rehabilitation technologies and practice. Specific research interests include functional electrical stimulation, activity-based neuromotor rehabilitation, neural coding, and neural control of prosthetic devices. His research has been supported by grants from the National Institute of Biomedical Imaging and Bioengineering (NIBIB), the National Institute of Neurological Diseases and Stroke (NINDS), the US Army's Telemedicine and Advanced Technology Research Center (TATRC), and the Defense Advanced Research Projects Agency (DARPA). He has been a member of IEEE and IEEE EMBS since 1994 and a member of the Society for Neuroscience since 1995.

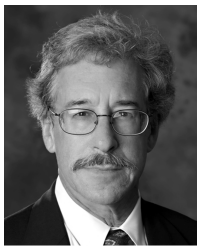

Gerald E. Loeb (M'98) received a B.A. ('69) and M.D. ('72) from Johns Hopkins University and did one year of surgical residency at the University of Arizona before joining the Laboratory of Neural Control at the National Institutes of Health (1973-1988). He was Professor of Physiology and Biomedical Engineering at Queen's University in Kingston, Canada (1988-1999) and is now Professor of Biomedical Engineering and Director of the Medical Device Development Facility at the University of Southern California. Dr. Loeb was one of the original developers of the cochlear implant to restore hearing to the deaf and was Chief Scientist for Advanced Bionics Corp. (1994-1999), manufacturers of the Clarion cochlear implant. He is a Fellow of the American Institute of Medical and Biological Engineers, holder of 52 issued US patents and author of over 200 scientific papers (available from http://bme.usc.edu/gloeb).